The quantum efficiency of pn-detectors from the near infrared to the soft X-ray region

R. Hartmann*, K.-H. Stephan, L. Strüder

Max-Planck-Institut für Extraterrestrische Physik, MPI Halbleiterlabor, Paul-Gerhardt-Allee 42, D-81245, Munchen, Germany

Abstract

The quantum efficiency of back-illuminated silicon pn-junction detectors is evaluated in the spectral range from 1.2 to 1400 eV, comprising the near infrared, visible, ultraviolet and soft X-ray regions. The calibrations are performed with the same device over the entire measured range, thus eliminating technological variations of the entrance window. Recent technological developments have yielded detectors with near-theoretical quantum efficiencies.

1. Introduction

Back-illuminated silicon pn-junction detectors have shown their suitability in many fields of application during the past years, just to mention the pn-CCD, which will contribute to the focal plane instrumentation of the X-ray Multi Mirror (XMM) and A Broad-band Imaging X-ray All-sky Survey (ABRIXAS) satellite missions, or the silicon drift detector, used as a versatile detector in many applications such as material research [1,2].

Outstanding characteristics of these detectors are their extended sensitivity to strong absorbing radiation in the ultraviolet (UV) and soft X-ray region. The spectral resolution for low-energy X-rays was significantly improved by the application of an ultra-shallow p^+ implantation at the rear contact, which acts as the radiation entrance window. Further technologies imply an additional n-implantation at the rear pn-junction to increase the electric field, well-defined annealing procedures to reform an almost perfect crystal lattice after ion-implantation and a thin, high-quality SiO_2 layer to reduce interface traps [3,4]. In combination with the large sensitive volume of 300 μm thickness, these detectors are able to efficiently detect radiation from the near infrared (IR) to the X-ray spectral region [5].

In this paper, we present the latest results of the quantum efficiency of these detectors. A pn-CCD with a sensitive area of $1 \times 3\ cm^2$ and a pixel size of $150 \times 150\ \mu m^2$ was used for measurements in the X-ray region. The detector, which consists of a sub-unit of the pn-CCD focal plane camera developed for the XMM and ABRIXAS satellite missions, was operated in a single-photon counting mode. For a determination of the quantum efficiency in the IR to vacuum ultraviolet (VUV) region,

the above-described pn-CCD was operated like a photodiode, measuring DC-photocurrents. Due to the concept of back-illumination, the different operating modes have no impact on the detector response. Signal electrons are collected at the n^+ substrate contact, which acts as the voltage reference point in a CCD operating mode.

2. Experimental methods

2.1. Near IR to VUV spectral region

The facility used for measurements in the range from 150 nm (8.2 eV) to 1000 nm (1.2 eV) consists of a Seya–Namioka monochromator and a wall-stabilized argon mini-arc light source [6]. The arc-source was operated at an electrical power of 2 kW. Special precautions were taken to reduce stray-light contributions in the UV-range below 1%. Measurements in the UV and VUV range were performed with a 1200 l/mm grating, while for wavelengths above 350 nm a 600 l/mm grating was applied. For a correct wavelength calibration of the monochromator, characteristic emission lines of dopand gases such as CO_2 and N_2 were used. The output radiant power was in the order of 0.5 to 100 nW on an illuminated area of $2 \times 2\ mm^2$. The determination of the absolute radiant power was done by two recently calibrated photodiodes (IRD AXUV-100 G for the UV range and HAMAMATSU S1337 at longer wavelengths).

Once a photon has passed the covering layers of the detector, the internal quantum efficiency (QE_{int}) physically describes the probability to register signal charges which are generated by the photon. Consequently, a non-perfect internal quantum efficiency accounts for trapping and recombination of signal charges in the detector bulk material and at its interface to the SiO_2 layer. The internal quantum efficiency of the detector is derived from the measured spectral responsitivity s by the following equation:

$$QE_{int} = \frac{hc}{e\lambda}\frac{s}{T} \tag{1}$$

where T denotes the transmittance of radiation through layers covering the detector entrance window. In the visible region, the transmittance T equals $1 - R$ (R: reflectance) of the detector surface layers. This is not valid anymore in the VUV-range. A significant fraction of the incoming radiation will be absorbed then. To account for both reflectance and absorptance, the Maxwell equations for electro-magnetic waves transversing a stack of adjacent layers at normal incidence were solved [7]. To confirm the calculations, the reflectance of our detector for normal incidence was determined by measurements. These experiments were performed at the radiometry laboratory of the Physikalisch-Technische Bundesanstalt (PTB) at the electron storage ring BESSY [8]. To protect the detector structures from possible radiation damages which might occur during reflectance measurements, an identical device from the same wafer was used instead.

When fitting the effect of a SiO_2 layer thickness for a simple SiO_2–Si interface to the measured reflectance data, the calculations do not fit the measurement data over the entire energy range. Deviations occur for wavelengths below 250 nm. It is necessary to pay special attention to the nature of a silicon–silicondioxide interface. Due to different lattice structures, the transition from crystalline silicon to a stoichiometrically correct SiO_2 takes several atomic layers, forming a SiO_x with x ranging from 0 to 2. Due to the lack of optical data for such a SiO_x formation, it was approximated by one SiO-layer. Assuming a thickness of 1.5 nm and a SiO_2-layer thickness of 30.5 nm, the measured reflectance data are fitted excellently within the entire range. Fig. 1 shows measured and calculated reflectance curves of our detector. Optical constants for calculations were taken from literature [9].

2.2. X-ray spectral region

Measurements in the energy range from 150 to 1400 eV were performed at the radiometry laboratory of the PTB at the electron storage ring BESSY in Berlin. At the SX-700 grazing-incidence monochromator, the electron current within the storage ring can be used as a reference for the photon flux at the monochromator exit slit [10]. The absolute number of photons per time unit and ring current

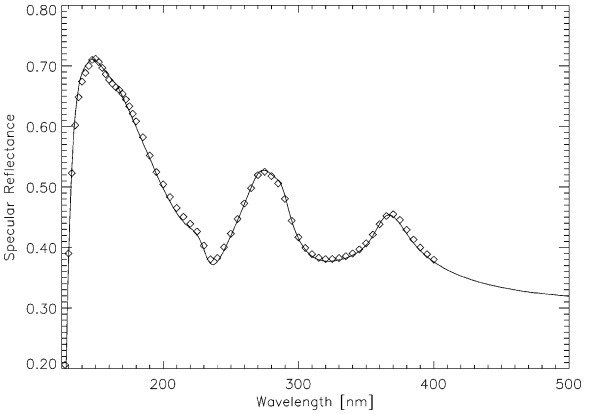

Fig. 1. Specular reflectance in the 120 to 500 nm spectral range. Measurements are indicated by diamonds. Calculations were done for an SiO_2 layer thickness of 30.5 plus 1.5 nm SiO. SiO gives a good optical approximation for the SiO_x layer at the transition from crystalline Si to SiO_2, which has a thickness of a few atomic layers.

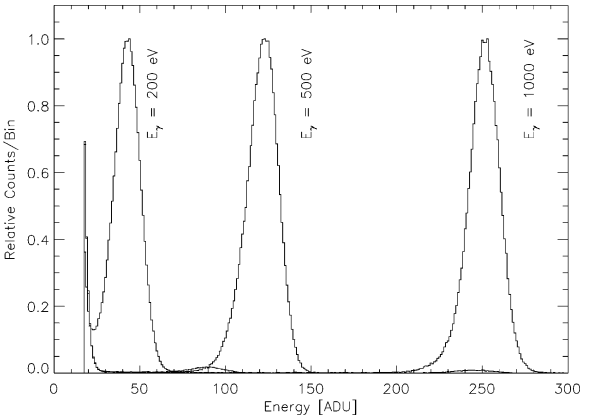

Fig. 2. Measured spectra of the pn-CCD to monoenergetic X-rays at 200 eV, 500 eV and 1 keV. Note that the three measurements were merged for this plot. Only single-pixel events were taken into account. The 200 eV measurement shows a pile-up peak of approximately 5% at an energy value of 90 ADU, while a minor pile-up peak is seen at around 245 ADU from the 500 eV measurement.

was determined before and after each measurement by a calibrated reference diode. During CCD measurements, a chopper wheel reducing the intensity by a factor of 10^{-4} was moved into the beam to arrive at a photon flux of approximately $800\,s^{-1}\,cm^{-2}$. The CCD readout cycle and the chopper wheel frequency were synchronized to make sure that no photons hit the CCD during readout time. The illuminated area was $40\,mm^2$. Depending on the photon flux, the measuring time per energy was between 30 and 50 minutes. More than half a million counts were accumulated in one spectrum.

Fig. 2 shows measured spectra of 200 eV, 500 eV and 1 keV, respectively, merged into one plot. Small asymmetries in the photo peak are due to the escape of fast signal electrons out of the sensitive detector volume and the recombination of signal electrons close to the detector surface. The linearity of the device is shown in Fig. 3. A single Gaussian model was applied to fit the peak position, disregarding any peak asymmetries caused by the entrance window. Shifts in the peak position occur either by charge losses close to the detector entrance window (recombination) or by non-linearities of the pair creation energy of silicon. Since no detector model was applied for the

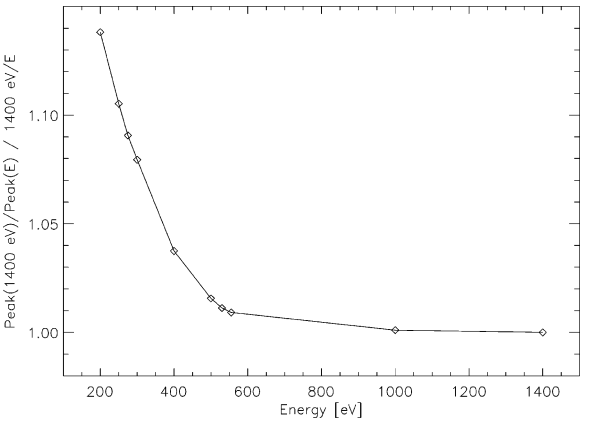

Fig. 3. Measured relative peak position as a function of incident photon energy, normalized to 1400 eV. Non-linearities occur due to loss of signal charge at the detector entrance window and variations of the mean pair creation energy of silicon for low-energy X-rays.

fitting of the peak position, the data give an upper limit for changes in the pair-creation energy of silicon.

The quantum efficiency was derived as the ratio of all reconstructed events during a certain period of time to the total number of incident photons. For a reconstruction of split events, a pattern recognition routine was used, which also eliminated

minimum ionizing particles being absorbed within the detector volume during measurement time [11].

3. Results

In the 950 to 300 nm spectral range, the internal quantum efficiency remains one (see Fig. 4), while for longer wavelengths a decrease is observed, as expected, due to radiation transversing the detector without interaction. The absorption length of silicon changes by more than four decades within this spectral region to values below 5 nm for a wavelength of 300 nm (4.1 eV). From examinations of the rear p^+-doping profile by secondary-ion mass spectroscopy (SIMS) and spreading resistance profile (SRP) measurements, the pn-junction may be derived to be placed at a depth of approximately 40 nm. A small surface recombination velocity and long diffusion length are required for the collection of signal electrons in the highly doped p^+-region. This is an indication of the high purity of our detector bulk material and well-annealed crystal lattice within the implanted region at the radiation entrance side.

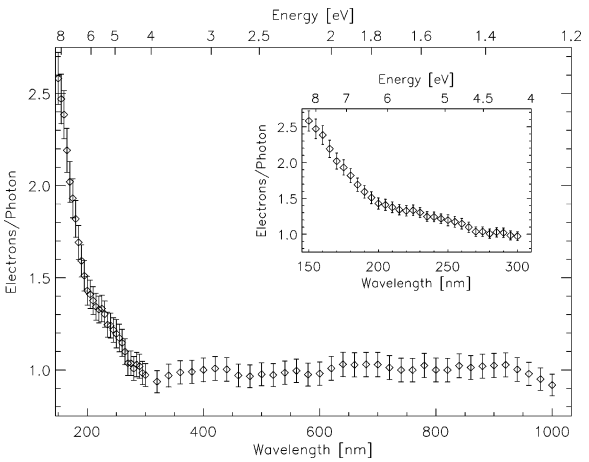

Fig. 4. Internal quantum efficiency in the wavelength range from 150 nm (8.3 eV) to 1000 nm (1.2 eV). Below 300 nm, a quantum yield is achieved. The drop beyond 950 nm is due to the beginning transparancy of silicon in the infrared.

Below 300 nm (4.1 eV) the quantum efficiency increases monotonously due to the onset of secondary ionization processes by primary generated photoelectrons [12]. At 150 nm (8.3 eV) a quantum yield of 2.6 is achieved. Unfortunately, measurement errors are dominated by the 1 sigma uncertainties in the reference diode calibrations, which account for 4–8%. More accurate measurements may be possible for example by recalibrating the reference diodes with an electrical substitution radiometer [13].

The quantum efficiency in the X-ray region is shown in Fig. 5. The drop in efficiency just above 500 eV is due to the oxygen absorption edge in the SiO_2 layer in the region above 536 eV. No drop in the efficiency is seen around the nitrogen edge, as expected, in contrast to front-illuminated CCDs, which often rely on silicon nitride for their pixel structures. Also shown is the pure absorption loss of photons in the covering SiO_2 layer thickness of 32 nm (including the transition layer between silicon and silicon dioxide). As already indicated by the spectral purity of low-energy spectra (see Fig. 2), internal losses of the detector material are small. Every photon being absorbed in the semiconductor is registered.

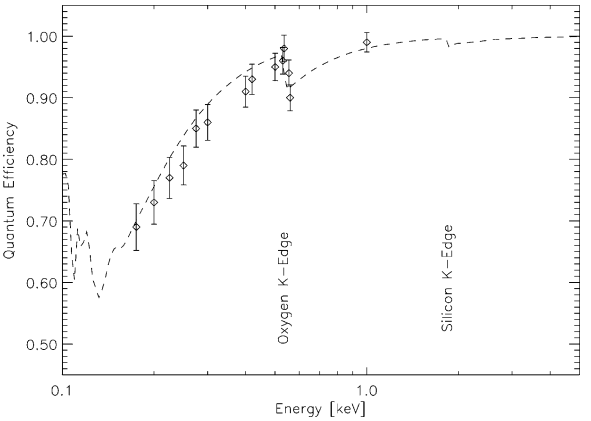

Fig. 5. Quantum efficiency of a pn-CCD in the X-ray region. The drop in the region above 536 eV is due to absorption in the covering SiO_2 layer. The estimation (dashed plot) is based on absorption losses in this covering layer only. Additional losses of the silicon detector itself cannot be observed within the uncertainties of the measurement. Every absorbed photon in the silicon crystal contributes to an observable signal of the detector.

4. Summary

The responsitivity of pn-detectors has been investigated in a wide spectral region. Correcting the measured data for reflectance and absorptance losses in the covering SiO_2 (and SiO_x) layers, near-theoretical internal quantum efficiencies are achieved in the IR to VUV spectral range. The same model describes the quantum efficiency in the X-ray region as well. The spectroscopic performance for low-energy X-rays is mostly limited by the amplifier noise and not by the radiation entrance window.

Both types of measurements coincide with respect to the minimal internal charge loss mechanisms of our detectors. Further research, however, is needed to obtain a correlation of the responsitivity in the UV-range and the shape of the X-ray photo peak in single-photon counting mode.

Improvements in the on-chip amplifier performance will allow one to perform measurements across the silicon L-edges in a single-photon counting mode, thus obtaining insight in fundamental solid-state properties of silicon.

Acknowledgements

The authors wish to thank all people who contributed to this paper, especially the technology staff of the semiconductor laboratory of the Max-Planck Institut and F. Scholze, M. Richter and U. Kroth of the Physikalisch-Technische Bundesanstalt in Berlin for their excellent support during our calibration campaigns. The assistance of W. Ertl of the Max-Planck Institut für Plasmaphysik concerning the argon mini-arc light source is gratefully acknowledged.

References

[1] P. Holl et al., IEEE Trans. Nucl. Sci. NS-45 (1998) 931.
[2] L. Strüder, R. Hartmann, P. Lechner et al., J. Synchrotron Rad. 5 (1998) 268.
[3] R. Hartmann, L. Strüder et al., Nucl. Instr. and Meth. A 377 (1996) 191.
[4] H. Soltau et al., Nucl. Instr. and Meth. A 439 (2000) 547.
[5] R. Hartmann, L. Strüder, E. Lorenz et al., Nucl. Instr. and Meth. A 387 (1997) 250.
[6] J.M. Bridges, W.R. Ott, Appl. Opt. 16 (1977) 367.
[7] S. Flügge, Handbuch der Physik, Vol. 24, Springer, 1956, p. 461.
[8] H. Rabus, V. Persch, G. Ulm, Appl. Opt. 36 (1997) 5421.
[9] E.D. Palik, Handbook of Optical Constants of Solids, Academic Press, San Diego, 1985.
[10] H. Rabus, F. Scholze, R. Thonagel, G. Ulm, Nucl. Instr. and Meth. A 377 (1996) 209.
[11] M. Popp et al., Nucl. Instr. and Meth. A 439 (2000) 567.
[12] S. Kolodinski, J.H. Werner, T. Wittchen, H.J. Queisser, Appl. Phys. Lett. 63 (1993) 2405.
[13] A. Lau-Främbs, U. Kroth, E. Tegeler, G. Ulm, Rev. Sci. Instr. 66 (1995) 2324.